Crossover designation recruits condensin to reorganize the meiotic chromosome axis

Victor A. Leon[1], Tovah E. Markowitz[1], Soogil Hong[2], Adhithi R. Raghavan[1], Jonna Heldrich[1], Keun Kim[2], and Andreas Hochwagen[1,*]

[1] Department of Biology, New York University; New York, NY; USA

[2] Department of Life Science, Chung-Ang University; Seoul; South Korea

[*] Correspondence: andi@nyu.edu

Running title: Role of condensin at crossover sites

Key words: Axial element, synapsis, ZMM factors, Pch2

Abstract

Crossover recombination supports meiotic chromosome inheritance and fertility by establishing chiasmata between homologous chromosomes prior to the first meiotic division. In addition to the physical exchange of DNA mediated by meiotic recombination, chiasma formation also involves restructuring of the underlying chromosome axis. Here, we identify condensin as an important regulator of axis remodeling in *S. cerevisiae*. Condensin is recruited near sites of meiotic crossover designation by pro-crossover factors but is largely dispensable for DNA exchange. Instead, condensin helps to create discontinuities in the meiotic chromosome axis. Condensin mutants exhibit significantly more continuous axis signals and exhibit a chromosomal buildup of the conserved axis remodeler Pch2. Consistent with an important role of axis restructuring at crossover sites, the canonical anaphase-bridge phenotype of condensin mutants is partly rescued by redirecting meiotic DNA repair to sister chromatids instead of homologous chromosomes, suggesting that crossover-associated axis reorganization is important for faithful meiotic chromosome segregation.

Introduction

Higher-order chromosome architecture allows cells to organize and maneuver large sections of chromatin to modulate gene expression, support DNA metabolism, and enable chromosome segregation [1,2]. The structural compartmentalization of chromosomes also plays a key role during meiotic recombination [3-5]. During early meiotic prophase I, chromosomes reorganize into linear arrays of chromatin loops along a protein-rich axis, known as the axial element. This loop-axis arrangement is of central importance for controlling meiotic recombination. It promotes recombination initiation by stimulating the formation of meiotic DNA double-strand breaks (DSBs), ensures the proper targeting of DSBs for homologous repair, and provides a platform for damage surveillance and checkpoint control [3,6]. In addition, the axial element serves as the foundation for the assembly of the synaptonemal complex (SC), a phase-separated, zipper-like structure that connects the axial elements of paired homologous chromosomes during the later stages of recombination [4,5]. Crossover intermediates mature in the context of the SC, ultimately leading to the physical exchange of DNA. SC formation, in turn, changes the axial elements, as several axial element proteins become depleted upon SC formation [7,8]. Notably, the axial element is also restructured locally at sites of crossover recombination [9]. In several systems, this local reorganization involves a cytologically apparent loss of sister chromatid cohesion [10-14] and presumably helps properly resolve and segregate exchange chromosome during the meiotic divisions. However, the mechanism underlying axial element reorganization in the vicinity of crossovers is not understood.

The chromosomal translocase condensin is a central regulator of higher-order chromosome organization in mitosis and meiosis [15,16]. Condensin belongs to the Structural Maintenance of Chromosomes (SMC) family of protein complexes, which can encircle chromatin through a ring-shaped binding interface, formed by two SMC ATPases and a kleisin linker protein. With the help of additional protein subunits, condensin, like other SMC complexes, promotes the ATP-dependent formation of DNA loops [17,18]. The budding yeast *S. cerevisiae* encodes a single condensin complex that consists of five subunits: the SMC proteins Smc2 and Smc4, the kleisin Brn1, as well as the Ycg1 and Ycs4 subunits.

Across eukaryotes, condensin is abundantly present on chromosomes at the time of meiotic recombination [19-22] but its function remains poorly understood. Condensin suppresses recombination of repetitive DNA in *S. cerevisiae* and *S. pombe* [23,24] and controls DSB distribution in *C. elegans* [25-27], but it is not required for normal DSB repair kinetics [19]. In late prophase I, condensin promotes reduction of another SMC complex, cohesin, from meiotic chromosomes [28], and helps in SC disassembly and chromosome individualization [25,29-31]. Similar to the characteristic mitotic chromosome bridging

observed in condensin mutants, meiotic chromosomes of condensin mutants also form bridges, in part because they are unable to sufficiently remove cohesin [19,28]. Intriguingly, the meiotic chromosome bridges of condensin mutants are also partly dependent on meiotic DSB formation [19], but the reason for this DSB-dependence has remained elusive.

Here, we further analyzed the function of condensin during meiotic prophase I in *S. cerevisiae*. We show that crossover designation triggers condensin enrichment near sites of crossover repair. Loss of condensin function led to more continuous axial elements, a higher level of cohesin at crossover-designated sites, and an accumulation of the axis remodeler Pch2. Importantly, targeting recombination events to sister chromatids rather than homologous chromosomes was sufficient to reduce anaphase bridges during meiosis I. Our data suggest that condensin-mediated reorganization of the axial element at sites of interhomolog recombination is important for meiotic chromosome segregation.

Results

Condensin binds to the axial element and DSB hotspots in response to recombination initiation

To define the mechanism of condensin accumulation on chromosomes during meiotic prophase I, we induced cultures to undergo a synchronous meiotic time course and analyzed the distribution of the condensin SMC subunit Smc4 fused to GFP on spread prophase chromosomes. In early prophase (2h), Smc4-GFP showed some foci on non-nucleolar chromatin but was primarily enriched in the nucleolus as indicated by a cluster of foci near the nucleolar marker Nop1 (**Fig. 1a-c**). As cells progressed into meiotic prophase (3h, 4h) and initiated SC formation, the nucleolar enrichment gradually weakened, and condensin formed numerous foci that localized on or near the SC protein Zip1 (**Fig. 1a**), consistent with prior analysis [19].

To identify chromosomal sequences enriched for condensin, we analyzed Smc4 functionally tagged with PK9 [32,33] by chromatin immunoprecipitation and sequencing (ChIP-seq). Synchronous cell populations were collected 3h after meiotic induction, corresponding to mid-prophase. Initial experiments using a standard ChIP-seq protocol failed to recover specific peaks of condensin enrichment when compared to a no-tag control (**Supplementary Fig. 1a**). The only exception was a specific peak in the rDNA (not shown). This recovery problem was meiosis-specific [33] and appeared to be linked to poor fragmentation of condensin-associated chromatin: proteolytic elimination of proteins after the immunoprecipitation step and re-sonication of the pure DNA fragments prior to library preparation [34] led to the recovery of

numerous specific peaks of Smc4-PK9 enrichment. These peaks were absent in a similarly treated control strain lacking the PK9 tag (**Supplementary Fig. 1a**).

Binding profiles of Smc4-PK9 from re-sonicated meiotic samples exhibited several features also seen for condensin in vegetative cells, including enrichment on the ribosomal DNA (rDNA), at tRNA genes, and around centromeres [32,35] (**Supplementary Fig. 1b-d**), as well as relative condensin accumulation between *CEN12* and the rDNA [33] (**Supplementary Fig. 1e**). In vegetative cells, condensin enrichment at pericentromeres and next to the rDNA is only observed during mitosis [32,36-38]. The appearance of similar enrichment in meiotic cells thus likely reflects the high degree of chromosomal compaction seen during meiotic prophase I [19]. Importantly, we observed uniquely meiosis-specific condensin enrichment, most prominently at sites of axial element attachment and at DSB hotspots (**Fig. 1d-e**). Axis attachment sites are defined by strong local enrichment of the meiosis-specific cohesin subunit Rec8 and the axial element factor Red1 [39-41]. Although Smc4-PK9 peaks visibly outnumbered the peaks of Rec8 and Red1, almost all axis Rec8 and Red1 peaks overlapped with Smc4-PK9 peaks (**Fig. 1d, Supplementary Fig. 1d)**. Many of the remaining meiosis-specific peaks localized to hotspots of DSB formation where condensin enrichment correlated broadly with hotspot activity (**Fig. 1f**) [42,43].

To directly test whether condensin binding is coordinated with meiotic recombination, we analyzed *spo11-Y135F* (*spo11-YF*) mutants, which lack catalytically active Spo11 nuclease and are unable to initiate meiotic DSB formation [44,45]. Although Smc4-GFP binding remained detectable on chromosomes in these mutants, the level of chromosomal association did not change over time and binding remained strong in the nucleolus (**Fig. 1b**). In addition, Smc4-PK9 binding to hotspots became nearly undetectable *spo11-YF* mutants (**Fig. 1f**), indicating that condensin enrichment on meiotic chromosomes depends on the initiation of meiotic recombination.

Recruitment of Smc4-GFP to meiotic chromosomes was also strongly reduced in *rec8* mutants (**Fig. 1b, e**), indicating that condensin recruitment depends on the presence of cohesin. Importantly, total signal intensity of chromosome spreads with detectable Smc4-GFP signal was not significantly different between wild type, *spo11-YF* mutants, and *rec8*Δ mutants at early time points (**Fig. 1c**), indicating that the changes in condensin patterns were primarily the result of condensin redistribution from the nucleolus to chromosomes. We conclude that meiotic DSB formation directs condensin enrichment towards the meiotic chromosomes, and that DSB hotspots and Rec8-dependent chromosome architecture provide binding sites for condensin upon DSB formation.

DSB-dependent condensin recruitment requires crossover designation but not synapsis

DSB formation triggers a series of changes along meiotic chromosomes that culminate in the formation of the SC [46,47]. Previous work had indicated that condensin remains bound to meiotic chromosomes in mutants lacking the SC transverse filament protein Zip1 [19]. However, as condensin redistribution coincided with the formation of the SC (**Fig. 1b**), we decided to revisit the possibility that condensin redistribution is linked to SC assembly. Analysis of *zip1*Δ mutants indeed showed some Smc4-GFP signal along Red1-decorated axial elements (**Fig. 2a**). However, unlike in wild-type cells, Smc4 also remained abundantly enriched in the nucleolus. In fact, the relative amounts of nucleolar and non-nucleolar staining were not significantly different between *zip1*Δ and *spo11-YF* mutants (**Fig. 2a**), indicating that the DSB-dependent redistribution of condensin from the nucleolus to chromosomes depends on Zip1.

Zip1 is a multifunctional protein that, in addition to supporting chromosome synapsis, also functions as part of the ZMM proteins to designate crossovers and protect nascent crossover repair intermediates from dissolution [48-51]. To test whether synapsis or crossover designation is required for condensin recruitment, we analyzed mutants that disrupt these processes individually. Smc4-GFP recruitment was unaltered in *ecm11*Δ mutants (**Fig. 2b**), which recombine normally but are unable to synapse chromosomes [52]. By contrast, condensin redistribution was equally strongly defective in another *zmm* mutant that is competent in forming some degree of SC (*zip3*Δ; **Fig. 2c**) Agarwal, 2000 #38}, indicating that condensin recruitment to meiotic chromosome arms requires ZMM-dependent crossover designation but not synapsis.

To determine whether condensin localizes to sites of crossover designation, we compared the distribution of Smc4-GFP with two ZMM factors, Msh4 and Zip3, both tagged with 13myc. Both proteins are well-established markers of crossover designation and repair [51,53,54]. We detected a large fraction of condensin foci at a consistent distance from Msh4 and Zip3 foci (**Fig. 3a-f**), whereas no such colocalization was observed when comparing Smc4-GFP with the axis remodeler Pch2, which also forms numerous foci along synapsed chromosomes (**Supplementary Fig. 2**) [55,56]. We conclude that ZMM factors are required for the recruitment of condensin near sites of crossover designation.

Condensin is not a ZMM factor

The ZMM-dependent recruitment of condensin raised the possibility that condensin itself functions as a ZMM factor. *zmm* mutants share several diagnostic phenotypes, including a strong arrest in meiotic prophase at high temperatures, reduced crossover formation, and increased non-crossover repair [49]. To test whether condensin is a ZMM factor, we analyzed meiotic progression of several temperature-sensitive condensin mutants. The mutants were allowed to enter the meiotic program at 25°C before shifting them to 34°C, the maximal temperature for normal meiotic progression in our strain background, around the time of early premeiotic S phase (1h time point). Both *ycg1-2* and *smc2-8* mutants efficiently completed meiosis at 25°C but were unable to form spores when shifted to 34°C (**Supplementary Fig. 3a-b**). *ycs4-2* cells already showed sporulation defects at room temperature, indicating that 25°C is partially restrictive for this mutant. By contrast, *smc4-1* mutants only showed a partial sporulation defect at 34°C, implying that *smc4-1* has a higher restrictive temperature (**Supplementary Fig. 3a-b**).

In line with the sporulation defect, condensin mutants at 34°C failed to properly separate DNA masses during the meiotic divisions (see e.g. **Supplementary Fig. 4e**), corroborating previous studies [19,28]. Importantly, however, condensin mutants formed the meiosis I spindle with wild-type kinetics at 34°C (**Supplementary Fig. 3b**). Thus, unlike *zmm* mutants, inactivation of condensin does not lead to a strong prophase arrest. The exception was *ycs4-2*, which showed asynchronous meiotic progression at both temperatures is likely due to defects originating in the preceding mitotic divisions, given the severity of this allele already at 25°C.

To further distinguish condensin from ZMM factors, we analyzed DSB formation and repair. Pulsed-field gel analysis revealed largely normal levels and distribution of meiotic DSBs in *ycg1-2* mutants along chromosome III (**Supplementary Fig. 3c**), in line with previous analyses of a major DSB hotspot [19]. At the model *HIS4LEU2* locus, DSB formation appeared slightly delayed in *ycg1-2* and *smc2-8* mutants (**Fig. 4a-b**). However, crossover repair progression, including single-end invasion, double-Holliday junction formation, and crossover resolution occurred at wild-type levels (**Fig. 4a, 4c-d, Supplementary Fig. 4**), and non-crossovers formation was similarly unaffected (**Fig. 4e-f**). Together, these data indicate that even though condensin requires ZMM factors for its recruitment near crossover sites, condensin itself is not a ZMM factor.

Condensin is required for normal meiotic axis morphogenesis

Our data suggests that condensin has functions near crossover-designated sites that are not related to DNA repair. To further investigate this possibility, we analyzed the morphology of crossover-designated sites in condensin mutants using Zip3-GFP. For these analyses, we also included a meiosis-specific depletion allele of *BRN1* (*brn1-mn;* [57]). The number of Zip3 foci remained largely unaltered in condensin mutants (**Supplementary Fig. 5a-b**), consistent with the overall normal levels of crossover formation. However, the size and intensity of Zip3 foci were significantly increased in the absence of condensin function (**Supplementary Fig. 5a, c-d**), indicating that condensin shapes the architecture of crossover-designated sites.

Previous work had indicated that condensin mutants are defective in SC formation [19]. However, those analyses were performed in cells after a prolonged prophase arrest, and the most severe mutant phenotype (*ycs4S*) was later attributed to a genetically linked variant in the promoter of *RED1* [58]. Therefore, we revisited SC formation in condensin mutants that were allowed to progress through meiosis with normal kinetics. We found that substantial SC formation occurred in all mutants as judged by the incorporation of the transverse filament protein Zip1 (**Fig. 5a**), although *ycs4-2* and *ycg1-2* exhibited mildly reduced SC length (**Fig. 5b**). In addition, all condensin mutants frequently exhibited Zip1 aggregates (polycomplexes), which are a sensitive indicator of synapsis defects (**Fig. 5c**) [59]. These findings indicate a mild defect in SC formation in the absence of condensin function.

The signals for Hop1 and Red1, which form the lateral elements of the SC, typically appear fragmented along synapsed chromosomes [7,60,61]. Analysis of Red1 staining in condensin mutants showed that lateral element fragmentation was significantly reduced, resulting in longer and fewer Red1 stretches (**Fig. 5a, d-e**). These data indicate that condensin is required to create discontinuities along the axes of synapsed chromosomes. In line with this interpretation, *zip3*Δ mutants, which fail to recruit condensin to crossover designated sites, also showed more continuous Red1 stretches (**Fig. 5f**). Furthermore, ChIP-seq analysis of the Red1 binding partner Hop1 showed only minor differences in the levels and chromosomal distribution of Hop1 (**Supplementary Fig. 6a-b**), as expected if the effects on the axis occur near crossover sites, which vary between cells.

The increased continuity of axial element staining in condensin mutants was associated with a pronounced increase in nuclei containing chromosomal DAPI signal in a characteristic "parallel track" arrangement (**Fig. 6a-b**). This arrangement is usually observed only transiently in wild-type nuclei. However, nucleus-wide parallel DAPI tracks are a feature of several chromosome remodeling mutants.

These include mutants in Pch2, which is responsible for extracting Hop1 and Red1 from chromosomes [7,60], as well as specific mutants in Zip1 and topoisomerase II (Top2) that are defective or delayed in Pch2 recruitment [7,62]. Therefore, we asked whether condensin mutants also fail to recruit Pch2. Contrary to this expectation, we observed a significant increase of Pch2 focus intensity on the chromosomes of condensin mutants (**Fig. 6c-e**). These findings indicate that the parallel track phenotype can be genetically separated from Pch2 recruitment. Although the increased Pch2 recruitment may hint that Pch2 cannot function properly in the absence of condensin, these data imply that the increased continuity of axial element signals in condensin mutants is not simply due to a failure to recruit Pch2.

Condensin reduces cohesin near sites of crossover designation

Condensin was previously shown to deplete Rec8-cohesin [28], which is the major recruiter of chromosomal Red1 [39,63,64]. Therefore, the breaks in Red1 continuity could be secondary to a local loss of Rec8 from synapsed chromosomes. In line with these observations, we found that Rec8 signal was consistently more continuous in condensin mutants, resulting in a reduced number of Rec8 stretches (**Fig. 7a-b**). Moreover, Rec8 staining at crossover-designated sites, marked by Zip3, was significantly lower in wild-type cells compared to condensin mutants (**Fig. 7c-d**). These data indicate that the altered Red1 distribution observed in condensin mutants is a consequence of defective remodeling of Rec8-cohesin and imply that condensin recruitment to crossover sites is important for restructuring the Rec8-dependent axial element.

Crossover-dependent chromosome bridging in condensin mutants

Chromosome bridging is a well-known phenotype of condensin mutants during mitotic cell division [16]. Intriguingly, bridging during meiotic anaphase I and II is partly dependent on meiotic DSB formation [19,28] (**Fig. 7e**), indicating that some of the bridging is a consequence of meiotic recombination. We considered the possibility that chromosome bridging is a result of defects in resolving double-Holliday junction intermediates into crossovers. However, double-Holliday junction resolution occurred normally in condensin mutants (**Fig. 4c**), indicating that the bridges are not caused by persistent joint molecules.

Nevertheless, the localization of condensin at sites of crossover repair suggested that the chromosome bridging may be linked to crossover formation. To test this possibility, we deleted the meiosis-specific checkpoint kinase Mek1. In *mek1* mutants, DSBs form normally but primarily use the sister chromatid as a repair template, leading to a profound drop in recombination between homologous chromosomes [65,66]. We found that deletion of *MEK1* reduced chromosome bridging in condensin mutants similarly to

spo11 mutants (**Fig. 7e**), indicating that part of the bridging phenotype arises from interhomolog recombination. Given that condensin removes cohesin (**Fig. 7a-b**)[28], we propose that the localized removal of cohesin around sites of crossover formation is essential for the separation of homologous chromosomes during the first meiotic division.

Discussion

Here, we demonstrate that condensin is recruited to designated crossover repair sites to regulate the meiotic chromosome axis. We propose that the function of meiotic condensin is to promote crossover-associated axis remodeling to ensure orderly separation of recombinant chromosomes during meiosis I.

Our data paint a dynamic picture of condensin localization that is in line with available data. Although condensin functions as a loop extruder, condensin tends to be more important for the timely remodeling of chromosomes than for stable chromatin loop formation. Many of condensin's roles align with this interpretation. For instance, condensin acutely relocalizes from the centromeres to chromosome arms during mitotic anaphase to help resolve sister chromatid entanglements [67,68], and from the nucleolus to meiotic centromeres to help co-orient sister kinetochores [57]. In addition, yeast condensin functions in the compaction and segregation of rDNA, clustering tRNA loci, and organizes a topologically associated domain specifically during anaphase [15,16]. Our data suggest that some of these activities also take place concurrently with meiotic recombination, perhaps explaining why a certain number of condensin foci are always detectable on meiotic chromosomes. However, overlaid over these background activities, we observed extensive redistribution of condensin from the nucleolus to sites of crossing over.

Which factors physically recruit condensin to crossover sites remains to be determined. One possibility is that components of the crossover machinery, such as the ZMM factors, directly bind condensin, thus coupling the assembly of crossover repair foci to the recruitment of condensin. Alternatively, condensin may recognize specific chromatin features that are unique to crossover repair intermediates. *In vitro*, condensin preferentially binds single-stranded DNA and can remove the single-stranded binding protein RPA [69,70]. Since extended RPA-coated D-loops are a feature of crossover intermediates [71], this structure could directly recruit condensin to crossover sites. Another possibility is that condensin is recruited by crossover-associated chromatin, similar to the recruitment of condensin to chromosome arms by histones H2A and H2A.Z during mitotic anaphase [68]. Although crossover-specific chromatin features have not yet been identified, several chromatin modifications are specifically detectable during meiotic

prophase [72-74] and could conceivably serve this function. A tight interaction of condensin with a larger crossover-associated intermediate or chromatin domain may also explain why ChIP-seq analysis of condensin required deproteination prior to re-sonication.

Even though condensin depends on and colocalizes with crossover repair factors, our data show no defects in crossover repair. Crossover levels are normal and no aberrant multi-chromatid structures were detected at the well-characterized *HIS4LEU2* hotspot. Moreover, crossover spacing (interference) was previously reported to be unaffected by condensin mutation [53]. These findings indicate that condensin is neither a pro-crossover ZMM factor [49] nor an anti-crossover factor, like the Sgs1 helicase [50,75]. Rather, the most prominent defects we observed were related to the aberrant structure of the meiotic chromosome axis, suggesting that condensin is primarily important for the axis reorganization near crossover sites.

Axis reorganization near crossover sites may be important for proper chromosome segregation for a couple of reasons. Crossover recombination can cause chromosomal interlocks, where chromosomes become trapped between pairs of synapsing chromosomes. If unresolved, these interlocks can in rare cases lead to aberrant chromosome alignment on the metaphase plate and result in mis-segregation [76]. Interlocks are abundant in mid-prophase but largely undetectable by late prophase [77,78], perhaps because of condensin activity. The timing of condensin recruitment to chromosomes is consistent with this hypothesis, as is the observation that interlock removal in *Arabidopsis thaliana* requires topoisomerase II [79], which often collaborates with condensin to promote chromosome organization. However, interlocks are infrequent in species with short chromosomes, such as budding yeast [13,80], and therefore cannot easily explain the scale of crossover-dependent chromosome bridging observed in condensin mutants. Furthermore, it is unclear why condensin would be enriched near crossover sites, as interlocks could essentially occur anywhere along chromosome arms.

Based on these considerations, we favor the model that condensin is necessary to remove crossover-associated cohesin domains. In organisms with suitable cytology, such as grasshoppers and different plants, local dissolution of sister chromatid cohesion around crossover sites is readily observable [10-12] and crossovers are sites of local Rec8 depletion in *Sordaria* and rat [13,14]. An overall condensin-dependent depletion of Rec8 from late meiotic prophase chromosomes has been reported in budding yeast [28,81,82], although whether this removal is linked to crossover sites was undetermined. Available data suggest that the pool of cohesin regulated by condensin is less sensitive to cleavage by separase [28],

leading us to speculate that the processes linked to crossover formation create separase-resistant cohesin domains. Such domains could be established through DNA damage-dependent recruitment of cohesin as has been observed in mitotic cells [83]. If this is the case, the bypass seen in *mek1* mutants may occur because DSBs are short-lived in this mutant [7,84], limiting extensive cohesin recruitment. Alternatively, crossover repair could induce local post-translational modification of cohesin. Intriguingly, phosphorylation of Rec8 by DDK was previously shown to regulate Rec8 prophase removal [81,82], and DDK function in meiotic prophase is at least partly regulated by Mek1 [85], potentially explaining the bypass we observed in *mek1* mutants. Thus, the establishment of separase-resistant cohesin domains may be temporarily important for supporting crossover repair but then needs to be reversed with the help of condensin before cells enter the first meiotic division to ensure controlled chromosome segregation.

Methods

Yeast strains and culture conditions

The strains utilized are listed in **Supplementary Table 1**. All strains are isogenic or congenic with the SK1 background. Gene disruption and tagging were carried out using a PCR-based protocol [86]. The Zip3-13myc and Zip3-GFP tags were provided by N. Kleckner and P. Jordan, respectively [53,87]. The Smc4-PK9 tag was transferred from W303 [32] using allele replacement by transformation. The Smc4-GFP tag is from [33] and the *pCLB2-BRN1* (*brn1-mn*) allele was described in [57]. The temperature-sensitive condensing alleles were introduced into SK1 by backcrossing a minimum of 7 times. The *ycg1-2* and *ycs4-2* alleles are from [19], *smc2-8* and *smc4-1* are from [88]. *smc2-8* is the result of an epitope tag within Smc2, as previously noted by [89]. To induce synchronous meiosis, strains were inoculated in BYTA for 16.5 hours at 30°C, washed two times with water and prepared for an OD_{600} = 2.0 at 30 °C in SPO medium [90]. Temperature sensitive strains were inoculated at OD_{600} = 0.3 in BYTA medium for 18 hours at 25°C and were inoculated in SPO medium at an OD_{600} = 2.0 at 25 °C for 1 hour before shifting to 34°C. For the experiments in **Fig. 4** and **Supplementary Fig. 4**, cells were pre-grown in YPA and shifted into SPM at 2.5h [91,92]. For all time courses, efficient meiotic entry was confirmed by monitoring DNA content using flow cytometry. Only cultures that efficiently entered meiosis were analyzed.

ChIP-seq analysis

Chromatin immunoprecipitation was performed as described [90]. For all ChIP-seq samples, 25mL meiotic culture were collected 3h after meiotic induction. Samples were immunoprecipitated with 2 µL anti-Red1 serum (Lot#16440, kind gift of N. Hollingsworth [84]), 2 µL anti-Rec8 serum and 2 uL anti-Hop1

serum (kind gift N. Hollingsworth [93]), 20µL anti-V5 (PK9) agarose affinity gel (Sigma) per IP. Library preparation was performed using Illumina TruSeq DNA Sample Prep Kits v1 but adapters were used at 1:20 dilution. Library quality was confirmed by Qubit HS assay kit and Agilent 2200 TapeStation. 150-bp sequencing was accomplished on an Illumina HiSeq 2500 or NextSeq 500 instrument. ChIP-seq data are averages of at least two biological replicates collected from samples grown on separate days and sequenced independently. The only experimental conditions with a single replicate were the no-tag control under traditional ChIP conditions and the ChIP of Hop1.

PK9 specific adjustments to ChIP-seq protocol

PK9 antibody binding is enriched at nucleosome-free regions and other open DNA in the no-tag controls, many of which are known condensin binding sites [32,89]. To increase the concentration of reads from longer ChIPed fragments, ChIP and input DNA were re-sonicated using a Bioruptor Pico (Diagenode, NJ, USA) with the following settings: 30 seconds ON and 30 seconds OFF for 5 cycles. This change to the general ChIP-seq protocol is not novel [94].

Data analysis

Sequencing reads were mapped to the SK1 genome [95] using Bowtie [96] and Bowtie2 [97]. Reads that mapped to only one location without mismatches were used in further analyses. Further processing was completed using MACS-2.1.0 (https://github.com/taoliu/MACS) [98]. Single end reads were extended towards 3' ends to a final length of 200 bp and probabilistically determined PCR duplicates were removed. Pileups of both the input and ChIP libraries were SPMR-normalized (signal per million reads), followed by a calculation of the fold-enrichment of the ChIP data over the input data. Before plotting, all data was normalized to produce a genome average of 1 to allow for some comparability between experiments. When available, reads of biological replicates were combined prior to MACS2 analysis. For analysis of the rDNA, reads were mapped to a single rDNA repeat using Bowtie with default settings.

Chromosome spreads

Meiotic nuclear spreads were performed as described [99]. GFP was detected using a polyclonal chicken anti-GFP antibody (abcam) at 1:100 dilution and an Alexa Fluor 488-conjugated anti-chicken secondary antibody at 1:200 dilution. Zip1 was detected using a polyclonal goat antibody against a C-terminal peptide of Zip1 (yC-19; Santa Cruz Biotechnology) at 1:200 and a Cy3-conjugated anti-goat secondary antibody at 1:200. Red1 was detected using rabbit serum (Lot#16440, kind gift of N. Hollingsworth [84] at

1:100 and Alexa 488-conjugated anti-rabbit secondary antibody at 1:200. Nop1 was detected using a mouse monoclonal Nop1 antibody (EnCor Biotechnology) at 1:400 and a Cy5-conjugated anti-mouse secondary antibody at 1:200. Rec8 was detected with a guinea pig anti-Rec8 serum (kind gift N. Hollingsworth [93]) at 1:400 and a Cy5-conjugated anti-guinea pig secondary antibody at 1:200. Pch2 was detected by using rabbit anti-Pch2 serum (kind gift from A. Shinohara [7]) and Alexa 488-conjugated anti-rabbit secondary antibody at 1:200. Myc-tagged proteins were detected using a mouse monoclonal anti-myc antibody (4A6; Millipore Sigma) and a Cy5-conjugated anti-mouse secondary antibody at 1:200. All secondary antibodies came from Jackson ImmunoResearch. Images were obtained on a Deltavision Elite imaging system (GE Applied Precision) adapted to an Olympus IX 17 microscope as described [99] and analyzed using softWoRx 5.0 and Fiji.

Colocalization analysis

Colocalization was analyzed in Fiji by utilizing the DiAna plugin for 3D localization and distance analysis [100]. A mask was created from the DAPI channel and regions of the DAPI signal that did not overlap with Zip1 were subtracted to exclude nucleolar condensin signals. This step was necessary because neither Zip3 nor Msh4 typically localizes within the nucleolus. Next, we processed the images with the DiAna plugin to quantify center-to-center distances between foci. To assess statistical spatial robustness, we performed a shuffle analysis with 100 iterations using the DiAna plugin, generating a uniform distribution representing predicted distances. The median focus distances per nucleus for the experimental and randomized datasets were used for statistical analysis.

Whole-cell immunofluorescence of spindles

A total of 300 uL was collected from a OD_{600} = 2.0 SPO medium, pelleted and fixed in formaldehyde as in [58]. Permeabilized cells were stained with monoclonal rat anti-tubulin antibody (YOL1/34; Santa Cruz Biotechnology) at 1:100 dilution and an Alexa Fluor 488-conjugated anti-rat secondary antibody (Jackson ImmunoResearch) at 1:200. DNA was visualized using DAPI mounting medium (VectaShield).

Pulsed-field gel electrophoresis and Southern analysis of chromosome III

For every time point, 10 mL of meiotic cultures from a OD_{600} = 2.0 SPO medium was collected and killed by adding sodium azide (0.1% final). Agarose plugs were prepared as in [90]. Plugs were melted and loaded into a 1.1% Seakem LE agarose gel and run in 0.5X TBE on CHEF Drive II apparatus (BioRad) using a 5 to 30 second ramp, run time 38h, voltage 5.4V/cm. After the run the DNA was stained with

ethidium bromide and exposed to UV light for 4 mins to fragment DNA. DNA was depurinated in 0.25 M HCl for 30 mins and denatured in 0.4M NaOH for 40 mins before transferring onto a HybondXL membrane (Cytiva) in 0.4M NaOH/0.6M NaCl overnight. The membrane was probed with and alpha-^{32}P-dCTP-labeled probe using a probe sequence near *MRC1* on chromosome III [101]. The membrane was exposed on Fujifilm imaging plates and images using a Typhoon FLA9000 instrument.

Analysis of recombination intermediates

Genomic DNA preparation and physical analysis were performed as described previously [91,92]. To synchronize yeast cell cultures, overnight YPD-cultured cells were transferred to SPS medium (1% potassium acetate, 1% bacteriological peptone, 0.5% yeast extract, 0.17% yeast nitrogen base with ammonium sulfate and without amino acids, 0.5% ammonium sulfate, 0.05 M potassium biphthalate, adjusted to pH 5.5 with 10 N KOH) and grown for 18 h at 25°C. Meiosis was induced by transferring the SPS-cultured cells to pre-warmed SPM medium (1% potassium acetate, 0.02% raffinose, two drops of Antifoam 204). SPM-cultured cells were harvested at 0, 2.5, 3.5, 4, 5, 6, 7, 8, 10 and 24 h after being transferred to the SPM medium and then cross-linked with psoralen under ultraviolet light at a wavelength of 360 nm. For the analysis of meiotic cells grown at 34◦C, cells were cultured at 25°C for up to 2.5 h and then shifted to 34°C in SPM medium. For 1D and interhomolog crossover (CO)/interhomolog noncrossover (NCO) gel analysis, 2 µg of genomic DNA was digested with XhoI and NgoMIV restriction enzymes. The digested DNA samples were loaded onto a 0.6% UltraKem LE agarose gel (Young Science, Y50004) in 1X TBE buffer and subjected to electrophoresis at ~2 V/cm for 24 hours. The DNA in the gel was stained with 0.5 µg/ml ethidium bromide (EtBr) for 30 minutes. For 2D gel analysis, 2.5 µg of genomic DNA was digested with XhoI and loaded onto a 0.4% Seakem Gold agarose gel (Lonza, 50152) in 1X TBE buffer. Electrophoresis was performed at ~1 V/cm for 21 hours. The gel was then stained with 0.5 µg/ml EtBr. For the second-dimension electrophoresis, gel strips were excised and placed onto a 2D gel tray, overlaid with 0.8% UltraKem LE agarose gel containing EtBr. Electrophoresis was conducted at ~6 V/cm at 4°C for 6 hours. For Southern blot analysis, hybridization was performed using 'Probe A,' which was labeled with ^{32}P-dCTP using a random primer DNA labeling kit (Enzynomics, EZ022S). Hybridization signals corresponding to Mom, Dad, DSBs, COs, SEIs, and dHJs were visualized using a phosphorimager and quantified using the Bio-Rad Quantity One software.

Acknowledgements

We thank F. Uhlmann, P. Jordan, N. Kleckner, H. Yu, and A. Strunnikov for sharing strains, N. Hollingsworth and A. Shinohara for sharing antibodies, and H. Murakami for helpful discussions. This work was supported in part through the NYU IT High Performance Computing resources, services, and staff expertise. We acknowledge the Zegar Family Foundation for their support. We thank the NYU Center for Genomics and Systems Biology Genomics Core for their assistance and resources. This work was supported by National Institutes of Health grant R35 GM148223 to AH and National Research Foundation of Korea (NRF) grant funded by the Korean government (MSIT) [RS-2023-00208191 to KPK]. ARR acknowledges support from a Fleur Strand Graduate Fellowship from the Department of Biology, as well as a Henry MacCracken Fellowship and a Dean's Dissertation Fellowship from the NYU Graduate School of Arts and Science. The funders had no role in the preparation of this manuscript.

Author contributions

Conceptualization, V.A.L, T.E.M, and A.H.; Investigation, V.A.L, T.E.M., S.H., A.R.R., J.H., K.P.K. and A.H.; Software, T.E.M.; Formal Analysis, V.A.L, T.E.M., S.H., A.R.R., J.H., K.P.K.; Writing – Original Draft, V.A.L., T.E.M, and A.H.; Writing – Review & Editing, V.A.L, T.E.M., S.H., A.R.R., J.H., K.P.K. and A.H.

Conflict of Interest

The authors declare no conflict of interest.

Data Availability

The datasets and computer code produced in this study are available in following databases:

- Meiotic ChIP-seq data: Gene Expression Omnibus (GEO) GSE154722 'https://www.ncbi.nlm.nih.gov/geo/query/acc.cgi?acc=GSE154722'
- Computer scripts for processing Illumina reads: Github 'https://github.com/hochwagenlab/ChIPseq_functions/tree/master/ChIPseq_Pipeline_v3/'
- Computer scripts for data analysis: Github 'https://github.com/hochwagenlab/condensin_recruitment/'

The analysis of condensin in asynchronous cells used previously published ChIP-seq data: GEO accession GSE106104 'https://www.ncbi.nlm.nih.gov/geo/query/acc.cgi?acc=GSE106104'

Figure legends

Figure 1. Condensin distribution on prophase chromosomes depends on *SPO11* and *REC8*.
(a) Representative images of Nop1 (red), Smc4-GFP (green), and Zip1 (orange) binding patterns on surface-spread nuclei, categorized as "No GFP", "Foci", "Foci & Cluster", or "Cluster" of GFP patterns. Bar = 1 µm. **(b)** Counts of GFP patterns on chromosome spreads in wild-type [H9443], *rec8*Δ [H9442], *spo11-YF* [H9441], or in the absence of a GFP tag ("no tag") [H7797], n=100. **(c)** Quantifications of GFP levels on nuclei from wild-type, *rec8*Δ, *spo11-YF*, and untagged control samples 3h after meiotic induction. Only nuclei with visible Zip1 staining were analyzed, n=25, 24, 27, 16 respectively. Total GFP intensity for each nucleus was normalized to background. Bars indicate mean and standard deviation (S.D). Wilcox test, (alternative hypothesis: greater). **(d)** Red1 (blue) [H119/6408] and Smc4-PK9 (pink) [H6408] binding pattern along chromosome II and a representative region (inset) in wild-type cells. Horizontal blue and pink lines represent genome average. **(e)** Heatmap of Smc4-PK9 enrichment around axis sites in wild type [H6408], and *rec8*Δ mutants [H7660]. Axis sites were defined as Red1 summits in wild-type cells with -log10 q-value greater than or equal to 20, as determined by MACS2. ChIP-seq values were averaged over 50bp windows around axis sites across a 3kb window. Rows are sorted by amount of Red1 binding at these sites. Heatmap colors represent enrichment (blue) or depletion (gold). Mean and 95% confidence intervals are shown in line graphs directly above heatmap. Gray line indicates mean and standard error of the mean (S.E.M.) from the no-tag controls [H7797, H8428]. **(f)** Heatmap of Smc4-PK9 enrichment around DSB hotspots in wild-type cells [H6408] and *spo11-YF* mutants [H8630]. Hotspots were placed into three quantiles grouped by strength (from hottest to weakest: maroon, pink, light blue). Hotspot locations and strengths derive from [43]. ChIP-seq values were averaged over 50bp windows around the midpoints of hotspots across a 3kb window. Rows in each quantile were sorted by Smc4-PK9 enrichment with pink indicating high enrichment and light blue indicating depletion. Mean and 95% confidence intervals are shown in line graph directly above the heatmap. Gray lines indicate mean and 95% confidence intervals of the no-tag controls [H7797, H8643]. The signal seen at hotspots in no-tag controls is because hotspots coincide with nucleosome-free regions, which fragment more frequently during sonication and thus create non-specific background signal.

Figure 2. Increased condensin binding to meiotic chromosomes requires crossover designation.
(a) Top: Representative images of Smc4-GFP (green) distribution on surface-spread nuclei from wild-type [H11471], *spo11-YF* [H9441], and *zip1*Δ mutants [H11499]. Chromosomes were also stained for

DNA (DAPI), Red1 (red), and the nucleolar marker Nop1 (blue). Nuclei were staged based on Red1 staining. Punctate Red1 staining was classified as leptonema and individualized Red1 axes were classified as pachynema (note that pachynema is defined by complete synapsis, which does not occur in *spo11-YF* and *zip1*Δ mutants; however, individualized Red1 axes are typically associated with pachynema in wild-type cells). Bar = 1 μm. **Bottom:** Smc4-GFP signal overlapping with Nop1 (nucleolar) or not overlapping with Nop1 (axial) was quantified. The percent of axial signal out of total signal is shown. Statistical significance was determined using Welch two-sample *t*-tests. **(b) Top:** Representative images of Smc4-GFP on spread wild-type [H11471] and *ecm11*Δ [H12818] **Bottom:** Quantification of wild-type [H11471] and *ecm11*Δ [H12818] nuclei during pachynema in (A). **(c) Top:** Representative images of Smc4-GFP on spread wild-type [H11471] and *zip3*Δ [H12925] nuclei during pachynema. Bottom: Quantification of wild-type [H11471] and *zip3*Δ [H12925] nuclei during pachynema as in (A).

Figure 3. Condensin is enriched near sites of crossover designation.

Representative images showing the relative distribution of Smc4-GFP (green) compared to **(a)** Zip3-13myc [H12926] or **(b)** Msh4-13myc [H11735] on surface-spread pachytene nuclei. DNA was stained with DAPI. nuc. = nucleolus, as apparent from the unsynapsed chromatin. **(c-d)** Distance analysis (DiAna) of Smc4-GFP and Zip3-13myc (c) and Msh4-13myc (d), respectively. The distances between nearest-neighbor foci were measured using focus centers. Bar graphs show the combined nearest-neighbor focus distances collected from the indicated number of nuclei. **(e-f)** Distribution of median focus distances per nucleus for Smc4/Zip3 focus pairs (e) and Smc4/Msh4 focus pairs (f). Input data is the same as for (c) and (d) and compared to matched randomized controls (see Methods). Wilcoxon rank sum exact test. Alternative: true location shift is not equal to 0.

Figure 4. Normal joint-molecule and crossover levels in condensin mutants.

(a) Temperature shift in SPM culture cells. The temperature in this experiment was increased from 25°C to 34°C after 2.5 hours. **(b)** Analysis of meiotic nuclear division: black rhombus represents wild-type [KKY4278], blue square represents *smc2-8* [KKY6547], and red circle represents *ycg1-2* [KKY6544]. **(c)** Representative 1D gel images of wild-type, *smc2-8*, and *ycg1-2* mutant strains. Double-strand break, DSB; joint molecules, JMs; crossovers, COs. **(d)** Quantification of DSB and CO species observed in (C). **(e)** Representative 2D gel images of wild-type, *smc2-8*, and *ycg1-2* mutant strains. **(f)** Quantification of SEI, IH-dHJ, and IS-dHJ species from (E). **(g)** Representative 1D gel images showing

interhomolog crossover (IH-CO) and interhomolog non-crossover (IH-NCO) in wild-type, *smc2-8*, and *ycg1-2* mutant strains. **(h)** Quantification of IH-COs and IH-NCOs from (G).

Figure 5. Meiotic chromosome axes are more continuous in condensin mutants.
Analysis of chromosome synapsis (Zip1) and chromosome axes (Red1) at pachynema in wild-type [H7797], *ycs4-2* [H8601], *ycg1-2* [H11281], *smc2-8* [H11364], and *brn1-mn* [H12022] mutants at 34°C. **(a)** Representative images showing the binding of Zip1 (red) and Red1 (green) in the indicated strains. DNA is stained with DAPI. Bar = 1 µm. **(b)** Quantification of total synapsis (Zip1 area) in the indicated strains. The number of analyzed nuclei is indicated. Wilcoxon rank sum test with continuity correction. **(c)** Incidence of Zip1 aggregates (polycomplexes) in the same nuclei as in (b). **(d)** Quantification of the average signal of individual Red1 stretches as a measure of axis fragment length. The number of analyzed nuclei is indicated. **(e)** Quantification of the total number of Red1 stretches per nucleus for the same nuclei as in (d). **(f)** Quantification of the total number of Red1 stretches at pachynema in wild-type [H11471] and *zip3Δ* mutants [H12925]. d-f: Wilcoxon rank sum test with continuity correction.

Figure 6. Abnormal chromatin morphology and Pch2 accumulation in condensin mutants.
(a) Representative images of chromatin morphology of spread pachytene chromosomes strained with DAPI in wild-type [H7797], *ycs4-2* [H8601], *ycg1-2* [H11281], and *smc2-8* [H11364] mutants at 34°C. Wild-type examples of nuclei with or without parallel DAPI tracks and *pch2Δ* mutants [H11758], which have strong parallel-track phenotype (Subramanian, MacQueen et al. 2016), are included for comparison (at 34°C). Bar = 1 µm. **(b)** Quantification of nuclei with predominantly parallel DAPI tracks in the indicated strains. **(c)** Representative images showing the relative binding of Pch2 (green) in the nucleolus (marked by staining with Nop1 in blue) and along the SC (marked by Zip1 in green) of spread pachytene chromosomes in wild-type [H7797], *ycs4-2* [H8601], *ycg1-2* [H11281], and *smc2-8* [H11364] and *brn1-mn* [H12022] mutants at 34°C. **(d)** Quantification of average Pch2 focus intensity on the indicated**. (e)** Quantification of the average Pch2 staining area per nucleus in the strains analyzed in (d). Wilcoxon rank sum test with continuity correction.

Figure 7. Continuous cohesin axes and interholomolog recombination-dependent meiotic missegregation in condensin mutants.
Analysis of Rec8 binding on spread pachytene chromosomes in wild-type [H7797], *ycs4-2* [H8601], *ycg1-2* [H11281], *smc2-8* [H11364], and *brn1-mn* [H12022] mutants at 34°C. **(a)** Representative images showing the binding of Zip1 (red) and Red1 (green) in the indicated strains. DNA is stained with DAPI.

Bar = 1 μm. **(b)** Quantification of the total number of Rec8 stretches per nucleus. The number of analyzed nuclei is indicated. **(c)** Analysis of Zip3-GFP (green) and Rec8 (red) binding on spread pachytene nuclei in wild-type [H13116], *ycg1-2* [H13117], *smc2-8* [H13118], and *brn1-mn* [H13141] mutants at 34°C. Bar = 1 μm. **(d)** Quantification of Rec8 signal overlapping with Zip3 foci in the indicated strains. The number of analyzed nuclei is indicated. Wilcoxon rank sum test with continuity correction. **(e)** Quantification of chromosome bridging in anaphase I and II nuclei in wild-type [H7797], *ycg1-2* [H11281], *smc2-8* [H11364], *spo11-YF* [H12173], *ycg1-2 spo11-YF* [H12227], *smc2-8 spo11-YF* [H12245], *mek1Δ* [H12137], *ycg1-2 mek1Δ* [H12194], *smc2-8 mek1Δ* [H12205]. The panels on the left show examples of spread nuclei with normal meiosis I chromosome separation or anaphase I chromosome bridging. DNA is stained with DAPI. The number of analyzed nuclei is indicated.

References

1 Hildebrand, E. M. & Dekker, J. Mechanisms and Functions of Chromosome Compartmentalization. *Trends Biochem Sci* **45**, 385-396 (2020). https://doi.org/10.1016/j.tibs.2020.01.002

2 Bickmore, W. A. & van Steensel, B. Genome architecture: domain organization of interphase chromosomes. *Cell* **152**, 1270-1284 (2013). https://doi.org/10.1016/j.cell.2013.02.001

3 Zickler, D. & Kleckner, N. Recombination, Pairing, and Synapsis of Homologs during Meiosis. *Cold Spring Harb Perspect Biol* **7** (2015). https://doi.org/10.1101/cshperspect.a016626

4 Borner, G. V., Hochwagen, A. & MacQueen, A. J. Meiosis in budding yeast. *Genetics* **225** (2023). https://doi.org/10.1093/genetics/iyad125

5 Ito, M. & Shinohara, A. Chromosome architecture and homologous recombination in meiosis. *Front Cell Dev Biol* **10**, 1097446 (2022). https://doi.org/10.3389/fcell.2022.1097446

6 Subramanian, V. V. & Hochwagen, A. The meiotic checkpoint network: step-by-step through meiotic prophase. *Cold Spring Harb Perspect Biol* **6**, a016675 (2014). https://doi.org/10.1101/cshperspect.a016675

7 Subramanian, V. V. *et al.* Chromosome Synapsis Alleviates Mek1-Dependent Suppression of Meiotic DNA Repair. *PLoS Biol* **14**, e1002369 (2016). https://doi.org/10.1371/journal.pbio.1002369

8 Wojtasz, L. *et al.* Mouse HORMAD1 and HORMAD2, two conserved meiotic chromosomal proteins, are depleted from synapsed chromosome axes with the help of TRIP13 AAA-ATPase. *PLoS Genet* **5**, e1000702 (2009). https://doi.org/10.1371/journal.pgen.1000702

9 Kleckner, N. Chiasma formation: chromatin/axis interplay and the role(s) of the synaptonemal complex. *Chromosoma* **115**, 175-194 (2006). https://doi.org/10.1007/s00412-006-0055-7

10 Petronczki, M., Siomos, M. F. & Nasmyth, K. Un menage a quatre: the molecular biology of chromosome segregation in meiosis. *Cell* **112**, 423-440 (2003).

11 Morgan, G. T. Absence of Chiasmata from Heteromorphic Region of Chromosome-I during Spermatogenesis in Triturus-Cristatus-Carnifex. *Chromosoma* **66**, 269-280 (1978). https://doi.org/Doi 10.1007/Bf00330555

12 Tease, C. & Jones, G. H. Analysis of Exchanges in Differentially Stained Meiotic Chromosomes of Locusta-Migratoria after Brdu-Substitution and Fpg Staining .1. Crossover Exchanges in Monochiasmate Bivalents. *Chromosoma* **69**, 163-178 (1978). https://doi.org/Doi 10.1007/Bf00329915

13 Storlazzi, A. *et al.* Recombination proteins mediate meiotic spatial chromosome organization and pairing. *Cell* **141**, 94-106 (2010). https://doi.org/10.1016/j.cell.2010.02.041

14 Eijpe, M., Offenberg, H., Jessberger, R., Revenkova, E. & Heyting, C. Meiotic cohesin REC8 marks the axial elements of rat synaptonemal complexes before cohesins SMC1beta and SMC3. *J Cell Biol* **160**, 657-670 (2003). https://doi.org/10.1083/jcb.200212080

15 Yatskevich, S., Rhodes, J. & Nasmyth, K. Organization of Chromosomal DNA by SMC Complexes. *Annu Rev Genet* **53**, 445-482 (2019). https://doi.org/10.1146/annurev-genet-112618-043633

16 Paul, M. R., Hochwagen, A. & Ercan, S. Condensin action and compaction. *Curr Genet* **65**, 407-415 (2019). https://doi.org/10.1007/s00294-018-0899-4

17 Hoencamp, C. & Rowland, B. D. Genome control by SMC complexes. *Nat Rev Mol Cell Biol* **24**, 633-650 (2023). https://doi.org/10.1038/s41580-023-00609-8

18 Kim, E., Barth, R. & Dekker, C. Looping the Genome with SMC Complexes. *Annu Rev Biochem* **92**, 15-41 (2023). https://doi.org/10.1146/annurev-biochem-032620-110506

19 Yu, H. G. & Koshland, D. E. Meiotic condensin is required for proper chromosome compaction, SC assembly, and resolution of recombination-dependent chromosome linkages. *J Cell Biol* **163**, 937-947 (2003). https://doi.org/10.1083/jcb.200308027
20 Chan, R. C., Severson, A. F. & Meyer, B. J. Condensin restructures chromosomes in preparation for meiotic divisions. *J Cell Biol* **167**, 613-625 (2004). https://doi.org/10.1083/jcb.200408061
21 Smith, S. J., Osman, K. & Franklin, F. C. The condensin complexes play distinct roles to ensure normal chromosome morphogenesis during meiotic division in *Arabidopsis*. *Plant J* **80**, 255-268 (2014). https://doi.org/10.1111/tpj.12628
22 Viera, A. *et al.* Condensin I reveals new insights on mouse meiotic chromosome structure and dynamics. *PLoS One* **2**, e783 (2007). https://doi.org/10.1371/journal.pone.0000783
23 Li, P., Jin, H. & Yu, H. G. Condensin suppresses recombination and regulates double-strand break processing at the repetitive ribosomal DNA array to ensure proper chromosome segregation during meiosis in budding yeast. *Mol Biol Cell* **25**, 2934-2947 (2014). https://doi.org/10.1091/mbc.E14-05-0957
24 Johansen, P. & Cam, H. P. Suppression of Meiotic Recombination by CENP-B Homologs in *Schizosaccharomyces pombe*. *Genetics* **201**, 897-904 (2015). https://doi.org/10.1534/genetics.115.179465
25 Hernandez, M. R. *et al.* Condensin I protects meiotic cohesin from WAPL-1 mediated removal. *PLoS Genet* **14**, e1007382 (2018). https://doi.org/10.1371/journal.pgen.1007382
26 Mets, D. G. & Meyer, B. J. Condensins regulate meiotic DNA break distribution, thus crossover frequency, by controlling chromosome structure. *Cell* **139**, 73-86 (2009). https://doi.org/10.1016/j.cell.2009.07.035
27 Lascarez-Lagunas, L. I. *et al.* Chromatin landscape, DSB levels, and cKU-70/80 contribute to patterning of meiotic DSB processing along chromosomes in *C. elegans*. *PLoS Genet* **19**, e1010627 (2023). https://doi.org/10.1371/journal.pgen.1010627
28 Yu, H. G. & Koshland, D. Chromosome morphogenesis: condensin-dependent cohesin removal during meiosis. *Cell* **123**, 397-407 (2005). https://doi.org/S0092-8674(05)00967-0
29 Hartl, T. A., Sweeney, S. J., Knepler, P. J. & Bosco, G. Condensin II resolves chromosomal associations to enable anaphase I segregation in *Drosophila* male meiosis. *PLoS Genet* **4**, e1000228 (2008). https://doi.org/10.1371/journal.pgen.1000228
30 Lee, J., Ogushi, S., Saitou, M. & Hirano, T. Condensins I and II are essential for construction of bivalent chromosomes in mouse oocytes. *Mol Biol Cell* **22**, 3465-3477 (2011). https://doi.org/10.1091/mbc.E11-05-0423
31 Resnick, T. D. *et al.* Mutations in the chromosomal passenger complex and the condensin complex differentially affect synaptonemal complex disassembly and metaphase I configuration in *Drosophila* female meiosis. *Genetics* **181**, 875-887 (2009). https://doi.org/10.1534/genetics.108.097741
32 D'Ambrosio, C. *et al.* Identification of *cis*-acting sites for condensin loading onto budding yeast chromosomes. *Genes Dev* **22**, 2215-2227 (2008). https://doi.org/10.1101/gad.1675708
33 Paul, M. R., Markowitz, T. E., Hochwagen, A. & Ercan, S. Condensin Depletion Causes Genome Decompaction Without Altering the Level of Global Gene Expression in *Saccharomyces cerevisiae*. *Genetics* **210**, 331-344 (2018). https://doi.org/10.1534/genetics.118.301217
34 Laczik, M. *et al.* Iterative Fragmentation Improves the Detection of ChIP-seq Peaks for Inactive Histone Marks. *Bioinform Biol Insights* **10**, 209-224 (2016). https://doi.org/10.4137/BBI.S40628
35 Wang, B. D., Eyre, D., Basrai, M., Lichten, M. & Strunnikov, A. Condensin binding at distinct and specific chromosomal sites in the *Saccharomyces cerevisiae* genome. *Mol Cell Biol* **25**, 7216-7225 (2005). https://doi.org/10.1128/MCB.25.16.7216-7225.2005

36 Verzijlbergen, K. F. *et al.* Shugoshin biases chromosomes for biorientation through condensin recruitment to the pericentromere. *eLife* **3**, e01374 (2014). https://doi.org/10.7554/eLife.01374
37 Lazar-Stefanita, L. *et al.* Cohesins and condensins orchestrate the 4D dynamics of yeast chromosomes during the cell cycle. *EMBO J* **36**, 2684-2697 (2017). https://doi.org/10.15252/embj.201797342
38 Schalbetter, S. A. *et al.* SMC complexes differentially compact mitotic chromosomes according to genomic context. *Nat Cell Biol* **19**, 1071-1080 (2017). https://doi.org/10.1038/ncb3594
39 Sun, X. *et al.* Transcription dynamically patterns the meiotic chromosome-axis interface. *eLife* **4**, e7424 (2015). https://doi.org/10.7554/eLife.07424
40 Glynn, E. F. *et al.* Genome-wide mapping of the cohesin complex in the yeast Saccharomyces cerevisiae. *PLoS Biol* **2**, E259 (2004). https://doi.org/10.1371/journal.pbio.0020259
41 Schalbetter, S. A., Fudenberg, G., Baxter, J., Pollard, K. S. & Neale, M. J. Principles of meiotic chromosome assembly revealed in *S. cerevisiae*. *Nat Commun* **10**, 4795 (2019). https://doi.org/10.1038/s41467-019-12629-0
42 Pan, J. *et al.* A hierarchical combination of factors shapes the genome-wide topography of yeast meiotic recombination initiation. *Cell* **144**, 719-731 (2011). https://doi.org/10.1016/j.cell.2011.02.009
43 Thacker, D., Mohibullah, N., Zhu, X. & Keeney, S. Homologue engagement controls meiotic DNA break number and distribution. *Nature* **510**, 241-246 (2014). https://doi.org/10.1038/nature13120
44 Bergerat, A. *et al.* An atypical topoisomerase II from archaea with implications for meiotic recombination. *Nature* **386**, 414-417 (1997).
45 Keeney, S., Giroux, C. N. & Kleckner, N. Meiosis-specific DNA double-strand breaks are catalyzed by Spo11, a member of a widely conserved protein family. *Cell* **88**, 375-384 (1997).
46 MacQueen, A. J. & Roeder, G. S. Fpr3 and Zip3 ensure that initiation of meiotic recombination precedes chromosome synapsis in budding yeast. *Curr Biol* **19**, 1519-1526 (2009).
47 Moens, P. B., Mowat, M., Esposito, M. S. & Esposito, R. E. Meiosis in a temperature-sensitive DNA-synthesis mutant and in an apomictic yeast strain (*Saccharomyces cerevisiae*). *Philos Trans R Soc Lond B Biol Sci* **277**, 351-358 (1977). https://doi.org/10.1098/rstb.1977.0023
48 Sym, M., Engebrecht, J. A. & Roeder, G. S. ZIP1 is a synaptonemal complex protein required for meiotic chromosome synapsis. *Cell* **72**, 365-378 (1993).
49 Borner, G. V., Kleckner, N. & Hunter, N. Crossover/noncrossover differentiation, synaptonemal complex formation, and regulatory surveillance at the leptotene/zygotene transition of meiosis. *Cell* **117**, 29-45 (2004).
50 Jessop, L., Rockmill, B., Roeder, G. S. & Lichten, M. Meiotic chromosome synapsis-promoting proteins antagonize the anti-crossover activity of sgs1. *PLoS Genet* **2**, e155 (2006). https://doi.org/10.1371/journal.pgen.0020155
51 Fung, J. C., Rockmill, B., Odell, M. & Roeder, G. S. Imposition of crossover interference through the nonrandom distribution of synapsis initiation complexes. *Cell* **116**, 795-802 (2004).
52 Humphryes, N. *et al.* The Ecm11-Gmc2 complex promotes synaptonemal complex formation through assembly of transverse filaments in budding yeast. *PLoS Genet* **9**, e1003194 (2013). https://doi.org/10.1371/journal.pgen.1003194
53 Zhang, L. *et al.* Topoisomerase II mediates meiotic crossover interference. *Nature* **511**, 551-556 (2014). https://doi.org/10.1038/nature13442
54 Agarwal, S. & Roeder, G. S. Zip3 provides a link between recombination enzymes and synaptonemal complex proteins. *Cell* **102**, 245-255 (2000).
55 San-Segundo, P. A. & Roeder, G. S. Pch2 links chromatin silencing to meiotic checkpoint control. *Cell* **97**, 313-324 (1999).

56 Joshi, N., Barot, A., Jamison, C. & Borner, G. V. Pch2 links chromosome axis remodeling at future crossover sites and crossover distribution during yeast meiosis. *PLoS Genet* **5**, e1000557 (2009). https://doi.org/10.1371/journal.pgen.1000557
57 Brito, I. L., Yu, H. G. & Amon, A. Condensins promote coorientation of sister chromatids during meiosis I in budding yeast. *Genetics* **185**, 55-64 (2010). https://doi.org/genetics.110.115139
58 Markowitz, T. E. *et al.* Reduced dosage of the chromosome axis factor Red1 selectively disrupts the meiotic recombination checkpoint in *Saccharomyces cerevisiae*. *PLoS Genet* **13**, e1006928 (2017). https://doi.org/10.1371/journal.pgen.1006928
59 Hughes, S. E. & Hawley, R. S. Alternative Synaptonemal Complex Structures: Too Much of a Good Thing? *Trends Genet* **36**, 833-844 (2020). https://doi.org/10.1016/j.tig.2020.07.007
60 Borner, G. V., Barot, A. & Kleckner, N. Yeast Pch2 promotes domainal axis organization, timely recombination progression, and arrest of defective recombinosomes during meiosis. *Proc Natl Acad Sci U S A* **105**, 3327-3332 (2008).
61 Smith, A. V. & Roeder, G. S. The yeast Red1 protein localizes to the cores of meiotic chromosomes. *J. Cell Biol.* **136**, 957-967 (1997). https://doi.org/10.1083/jcb.136.5.957
62 Heldrich, J., Sun, X., Vale-Silva, L. A., Markowitz, T. E. & Hochwagen, A. Topoisomerases Modulate the Timing of Meiotic DNA Breakage and Chromosome Morphogenesis in Saccharomyces cerevisiae. *Genetics* **215**, 59-73 (2020). https://doi.org/10.1534/genetics.120.303060
63 Klein, F. *et al.* A central role for cohesins in sister chromatid cohesion, formation of axial elements and recombination during yeast meiosis. *Cell* **98**, 91-103 (1999). https://doi.org/10.1016/S0092-8674(00)80609-1
64 Heldrich, J. *et al.* Two pathways drive meiotic chromosome axis assembly in Saccharomyces cerevisiae. *Nucleic Acids Res* **50**, 4545-4556 (2022). https://doi.org/10.1093/nar/gkac227
65 Niu, H. *et al.* Mek1 kinase is regulated to suppress double-strand break repair between sister chromatids during budding yeast meiosis. *Mol Cell Biol* **27**, 5456-5467 (2007). https://doi.org/MCB.00416-07
66 Niu, H. *et al.* Partner Choice during Meiosis Is Regulated by Hop1-promoted Dimerization of Mek1. *Mol Biol Cell* **16**, 5804-5818 (2005).
67 Leonard, J. *et al.* Condensin Relocalization from Centromeres to Chromosome Arms Promotes Top2 Recruitment during Anaphase. *Cell Rep* **13**, 2336-2344 (2015). https://doi.org/10.1016/j.celrep.2015.11.041
68 Tada, K., Susumu, H., Sakuno, T. & Watanabe, Y. Condensin association with histone H2A shapes mitotic chromosomes. *Nature* **474**, 477-483 (2011). https://doi.org/10.1038/nature10179
69 Sutani, T. & Yanagida, M. DNA renaturation activity of the SMC complex implicated in chromosome condensation. *Nature* **388**, 798-801 (1997). https://doi.org/10.1038/42062
70 Akai, Y. *et al.* Opposing role of condensin hinge against replication protein A in mitosis and interphase through promoting DNA annealing. *Open Biol* **1**, 110023 (2011). https://doi.org/10.1098/rsob.110023
71 Joo, J. H. *et al.* RPA interacts with Rad52 to promote meiotic crossover and noncrossover recombination. *Nucleic Acids Res* **52**, 3794-3809 (2024). https://doi.org/10.1093/nar/gkae083
72 Hsu, J. Y. *et al.* Mitotic phosphorylation of histone H3 is governed by Ipl1/aurora kinase and Glc7/PP1 phosphatase in budding yeast and nematodes. *Cell* **102**, 279-291 (2000). https://doi.org/10.1016/s0092-8674(00)00034-9
73 Hu, J. *et al.* H4K44 Acetylation Facilitates Chromatin Accessibility during Meiosis. *Cell Rep* **13**, 1772-1780 (2015). https://doi.org/10.1016/j.celrep.2015.10.070
74 Kar, F. M., Vogel, C. & Hochwagen, A. Meiotic DNA breaks activate a streamlined phospho-signaling response that largely avoids protein-level changes. *Life Sci Alliance* **1**, e202201454 (2022).

75 Oh, S. D. *et al.* BLM ortholog, Sgs1, prevents aberrant crossing-over by suppressing formation of multichromatid joint molecules. *Cell* **130**, 259-272 (2007).
76 Yacobi, Y. Z., Mellosampayo, T. & Feldman, M. Genetic Induction of Bivalent Interlocking in Common Wheat. *Chromosoma* **87**, 165-175 (1982). https://doi.org/Doi 10.1007/Bf00338487
77 Wang, C. J., Carlton, P. M., Golubovskaya, I. N. & Cande, W. Z. Interlock formation and coiling of meiotic chromosome axes during synapsis. *Genetics* **183**, 905-915 (2009). https://doi.org/10.1534/genetics.109.108688
78 Zickler, D. & Kleckner, N. Meiotic chromosomes: integrating structure and function. *Annu. Rev. Genet.* **33**, 603-754 (1999). https://doi.org/10.1146/annurev.genet.33.1.603
79 Martinez-Garcia, M. *et al.* TOPII and chromosome movement help remove interlocks between entangled chromosomes during meiosis. *J Cell Biol* **217**, 4070-4079 (2018). https://doi.org/10.1083/jcb.201803019
80 Rasmussen, S. W. & Holm, P. B. Mechanics of meiosis. *Hereditas* **93**, 187-216 (1980). https://doi.org/10.1111/j.1601-5223.1980.tb01360.x
81 Challa, K. *et al.* Meiosis-specific prophase-like pathway controls cleavage-independent release of cohesin by Wapl phosphorylation. *PLoS Genet* **15**, e1007851 (2019). https://doi.org/10.1371/journal.pgen.1007851
82 Challa, K., Shinohara, M. & Shinohara, A. Meiotic prophase-like pathway for cleavage-independent removal of cohesin for chromosome morphogenesis. *Curr Genet* **65**, 817-827 (2019). https://doi.org/10.1007/s00294-019-00959-x
83 Unal, E. *et al.* DNA damage response pathway uses histone modification to assemble a double-strand break-specific cohesin domain. *Mol Cell* **16**, 991-1002 (2004).
84 Wan, L., de los Santos, T., Zhang, C., Shokat, K. & Hollingsworth, N. M. Mek1 kinase activity functions downstream of *RED1* in the regulation of meiotic double strand break repair in budding yeast. *Mol Biol Cell* **15**, 11-23 (2004).
85 Chen, X. *et al.* Phosphorylation of the Synaptonemal Complex Protein Zip1 Regulates the Crossover/Noncrossover Decision during Yeast Meiosis. *PLoS Biol* **13**, e1002329 (2015). https://doi.org/10.1371/journal.pbio.1002329
86 Longtine, M. S. *et al.* Additional modules for versatile and economical PCR-based gene deletion and modification in *Saccharomyces cerevisiae*. *Yeast* **14**, 953-961 (1998).
87 Copsey, A. *et al.* Smc5/6 coordinates formation and resolution of joint molecules with chromosome morphology to ensure meiotic divisions. *PLoS Genet* **9**, e1004071 (2013). https://doi.org/10.1371/journal.pgen.1004071
88 Freeman, L., Aragon-Alcaide, L. & Strunnikov, A. The condensin complex governs chromosome condensation and mitotic transmission of rDNA. *J Cell Biol* **149**, 811-824 (2000). https://doi.org/10.1083/jcb.149.4.811
89 Murillo-Pineda, M., Cabello-Lobato, M. J., Clemente-Ruiz, M., Monje-Casas, F. & Prado, F. Defective histone supply causes condensin-dependent chromatin alterations, SAC activation and chromosome decatenation impairment. *Nucleic Acids Res* **42**, 12469-12482 (2014). https://doi.org/10.1093/nar/gku927
90 Blitzblau, H. G., Chan, C. S., Hochwagen, A. & Bell, S. P. Separation of DNA replication from the assembly of break-competent meiotic chromosomes. *PLoS Genet* **8**, e1002643 (2012). https://doi.org/10.1371/journal.pgen.1002643
91 Kim, K. P. *et al.* Sister cohesion and structural axis components mediate homolog bias of meiotic recombination. *Cell* **143**, 924-937 (2010). https://doi.org/10.1016/j.cell.2010.11.015
92 Hong, S. *et al.* The logic and mechanism of homologous recombination partner choice. *Mol Cell* **51**, 440-453 (2013). https://doi.org/10.1016/j.molcel.2013.08.008

93 Prugar, E., Burnett, C., Chen, X. & Hollingsworth, N. M. Coordination of Double Strand Break Repair and Meiotic Progression in Yeast by a Mek1-Ndt80 Negative Feedback Loop. *Genetics* **206**, 497-512 (2017). https://doi.org/10.1534/genetics.117.199703

94 Mokry, M. *et al.* Efficient double fragmentation ChIP-seq provides nucleotide resolution protein-DNA binding profiles. *PLoS One* **5**, e15092 (2010). https://doi.org/10.1371/journal.pone.0015092

95 Yue, J. X. *et al.* Contrasting evolutionary genome dynamics between domesticated and wild yeasts. *Nat Genet* **49**, 913-924 (2017). https://doi.org/10.1038/ng.3847

96 Langmead, B., Trapnell, C., Pop, M. & Salzberg, S. L. Ultrafast and memory-efficient alignment of short DNA sequences to the human genome. *Genome Biol* **10**, R25 (2009). https://doi.org/10.1186/gb-2009-10-3-r25

97 Langmead, B. & Salzberg, S. L. Fast gapped-read alignment with Bowtie 2. *Nat Methods* **9**, 357-359 (2012). https://doi.org/10.1038/nmeth.1923

98 Zhang, Y. *et al.* Model-based analysis of ChIP-Seq (MACS). *Genome Biol* **9**, R137 (2008). https://doi.org/10.1186/gb-2008-9-9-r137

99 Subramanian, V. V. *et al.* Persistent DNA-break potential near telomeres increases initiation of meiotic recombination on short chromosomes. *Nat Commun* **10**, 970 (2019). https://doi.org/10.1038/s41467-019-08875-x

100 Gilles, J. F., Dos Santos, M., Boudier, T., Bolte, S. & Heck, N. DiAna, an ImageJ tool for object-based 3D co-localization and distance analysis. *Methods* **115**, 55-64 (2017). https://doi.org/10.1016/j.ymeth.2016.11.016

101 Blitzblau, H. G., Bell, G. W., Rodriguez, J., Bell, S. P. & Hochwagen, A. Mapping of meiotic single-stranded DNA reveals double-strand-break hotspots near centromeres and telomeres. *Curr Biol* **17**, 2003-2012 (2007). https://doi.org/10.1016/j.cub.2007.10.066

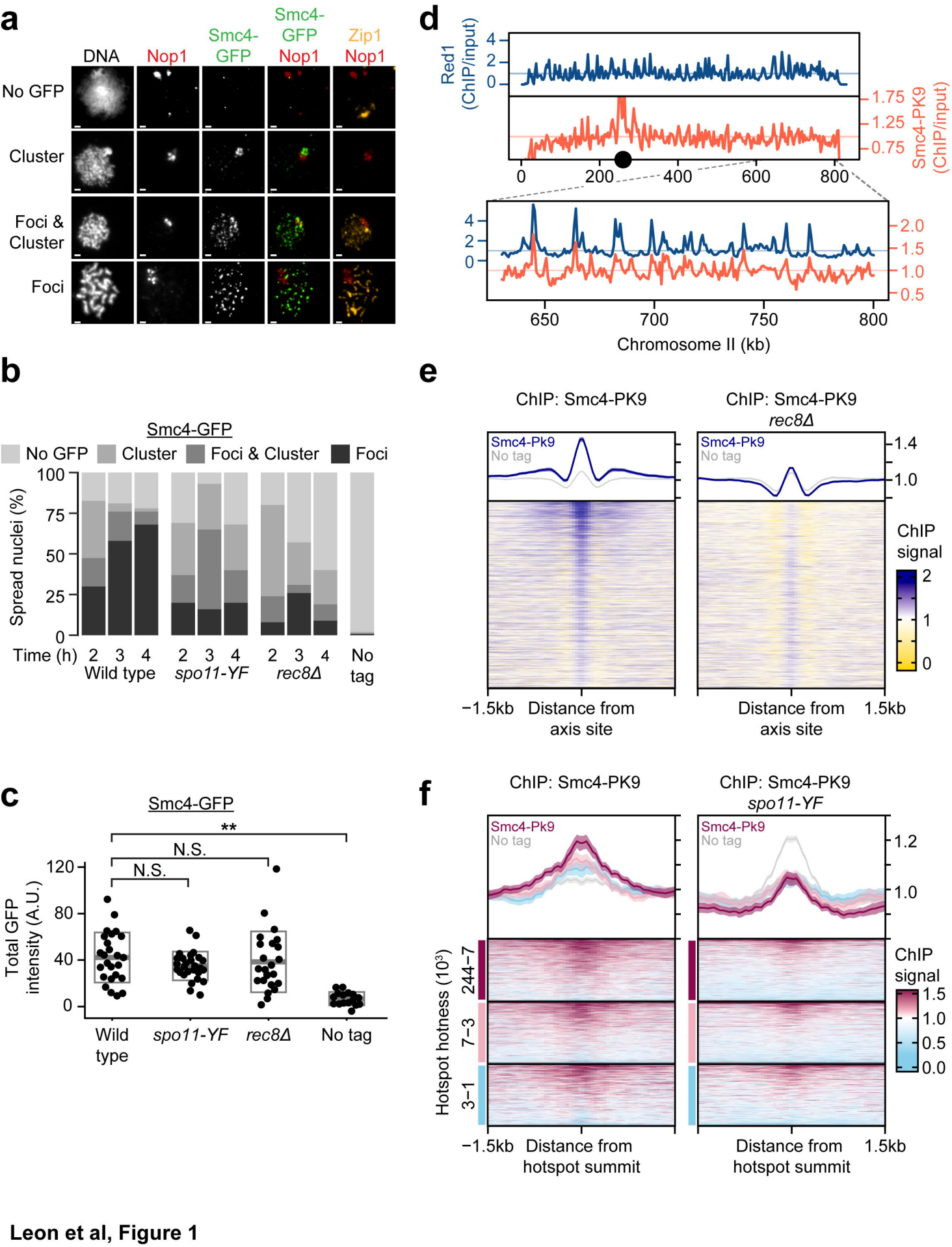

Leon et al, Figure 1

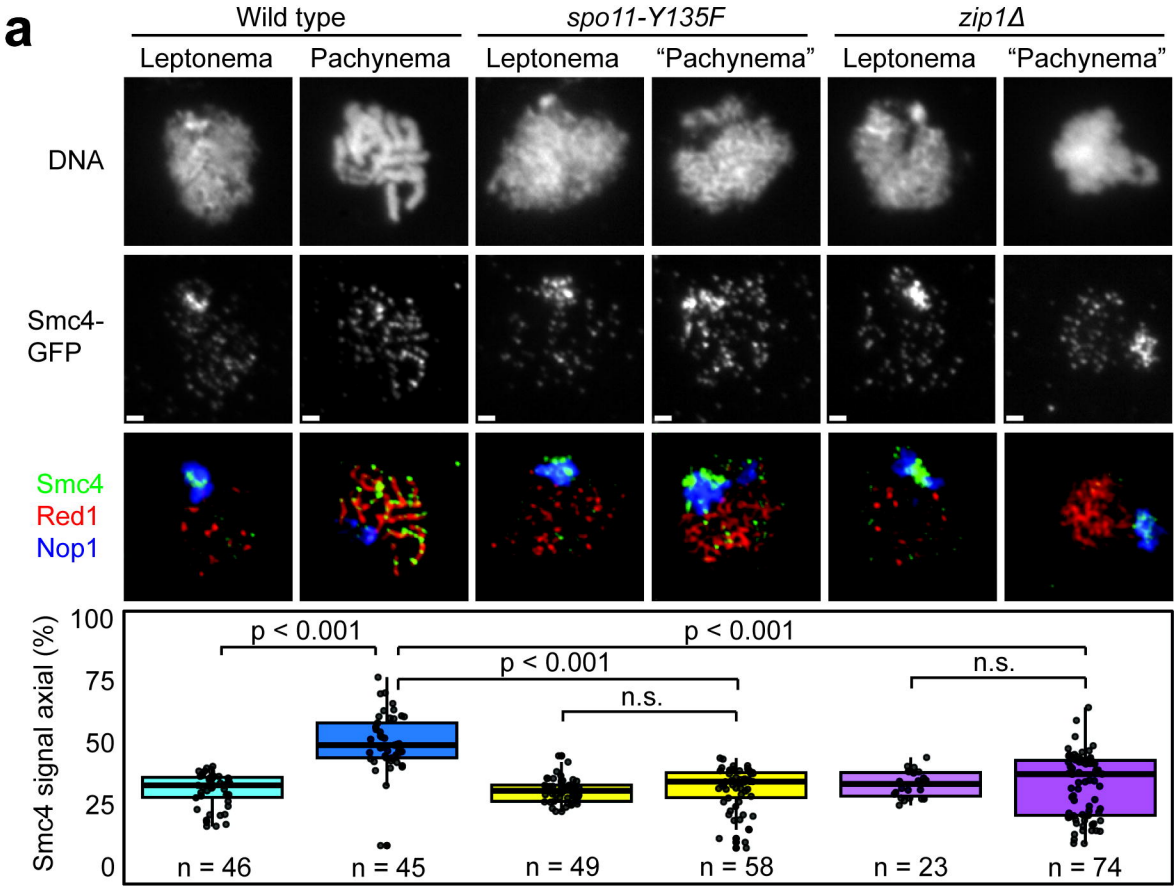

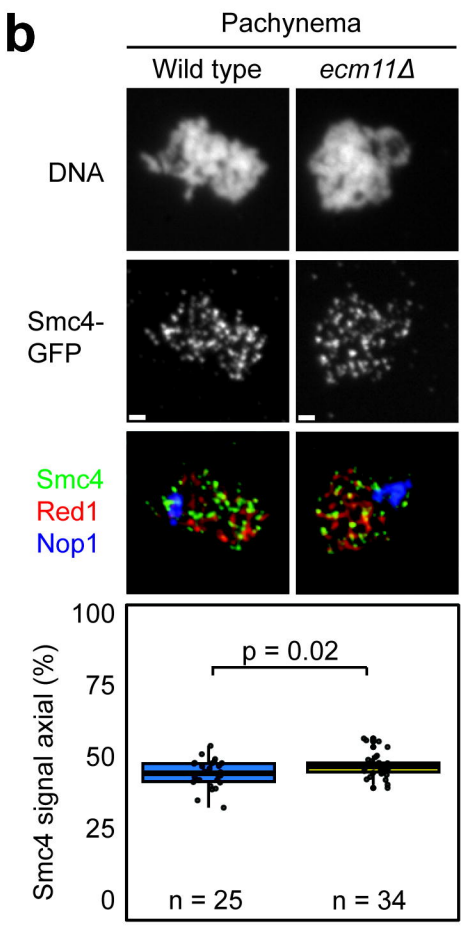

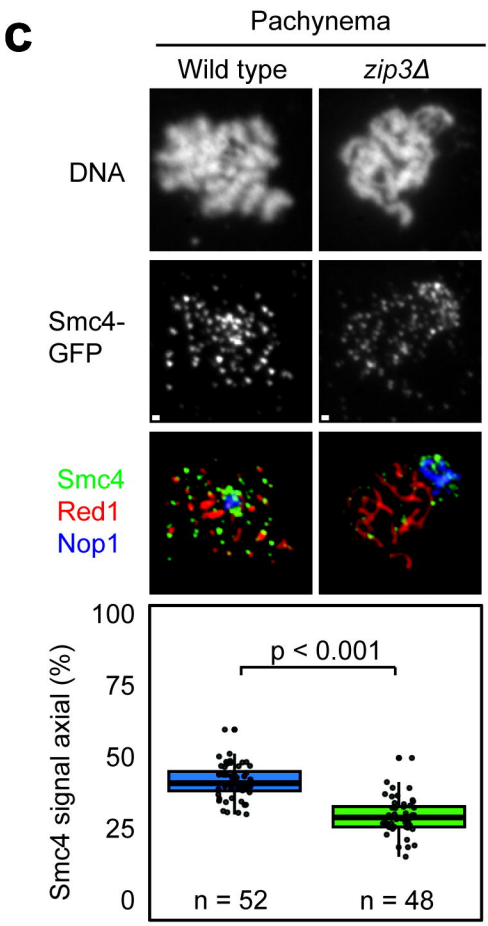

Leon et al, Figure 2

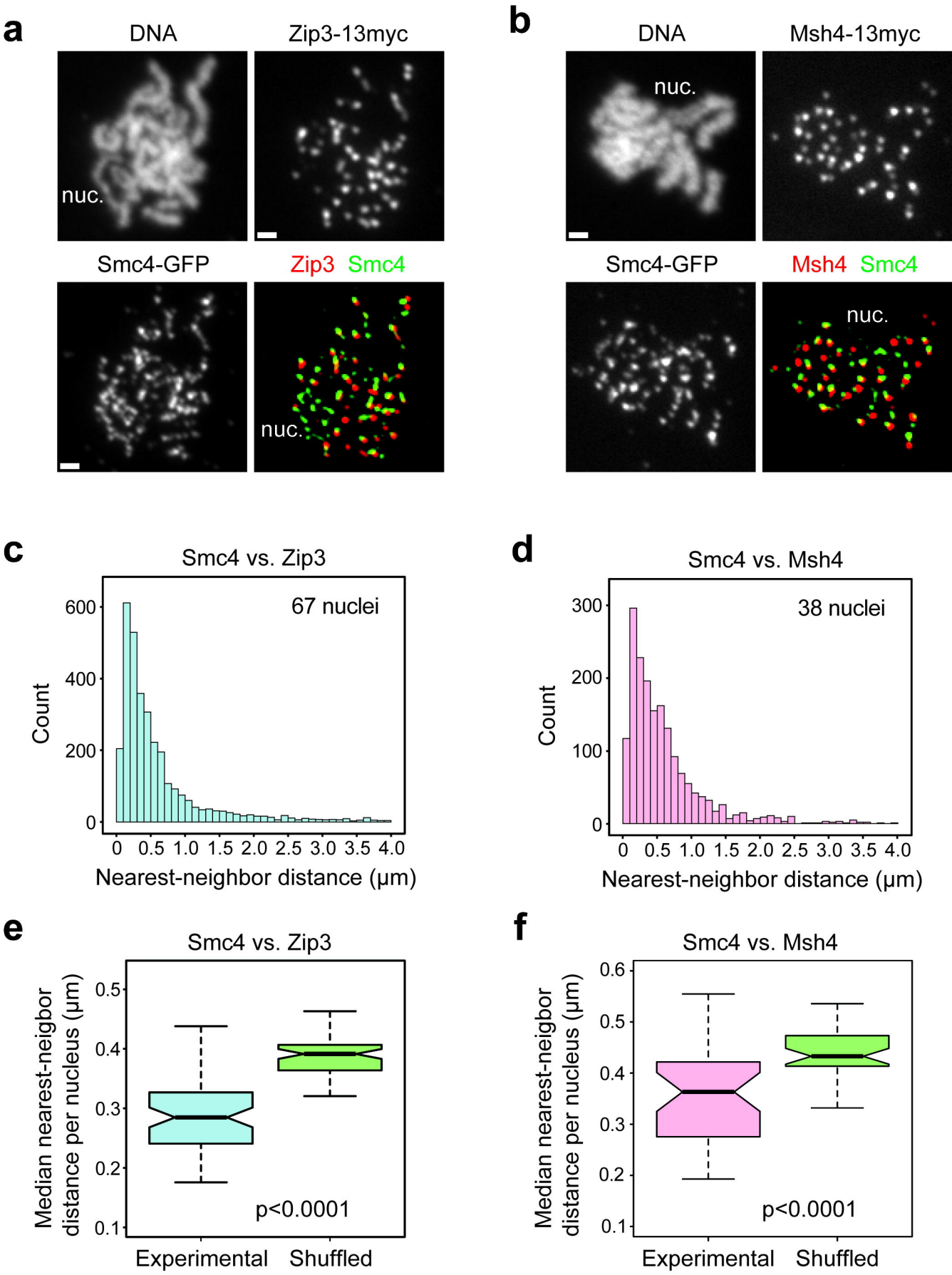

Leon et al, Figure 3

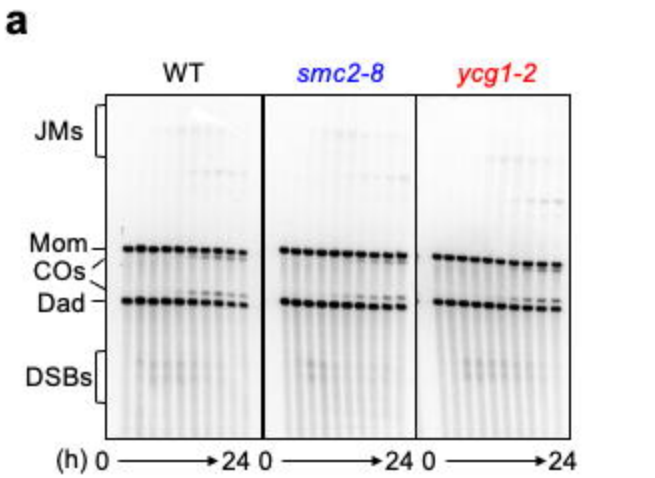

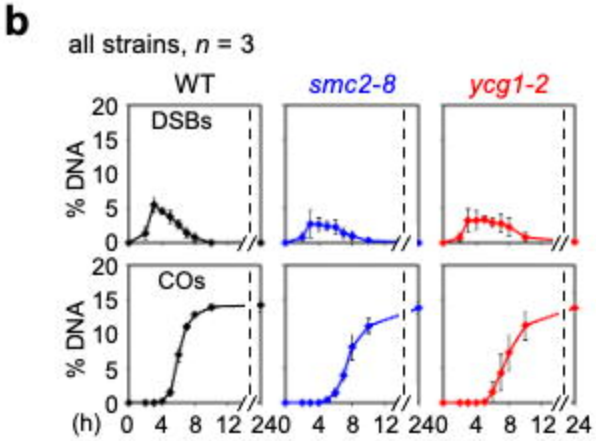

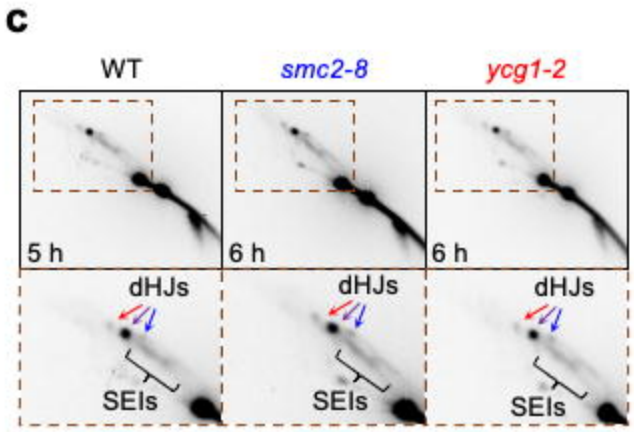

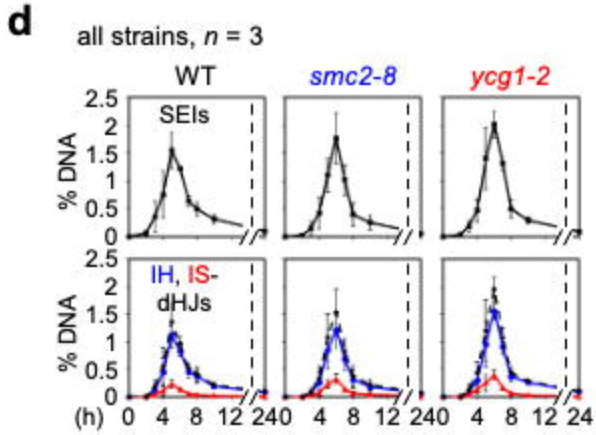

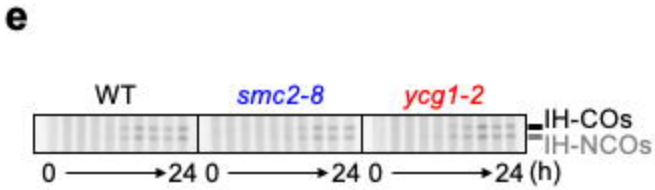

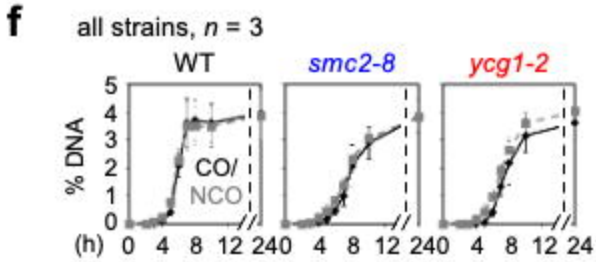

Leon et al, Figure 4

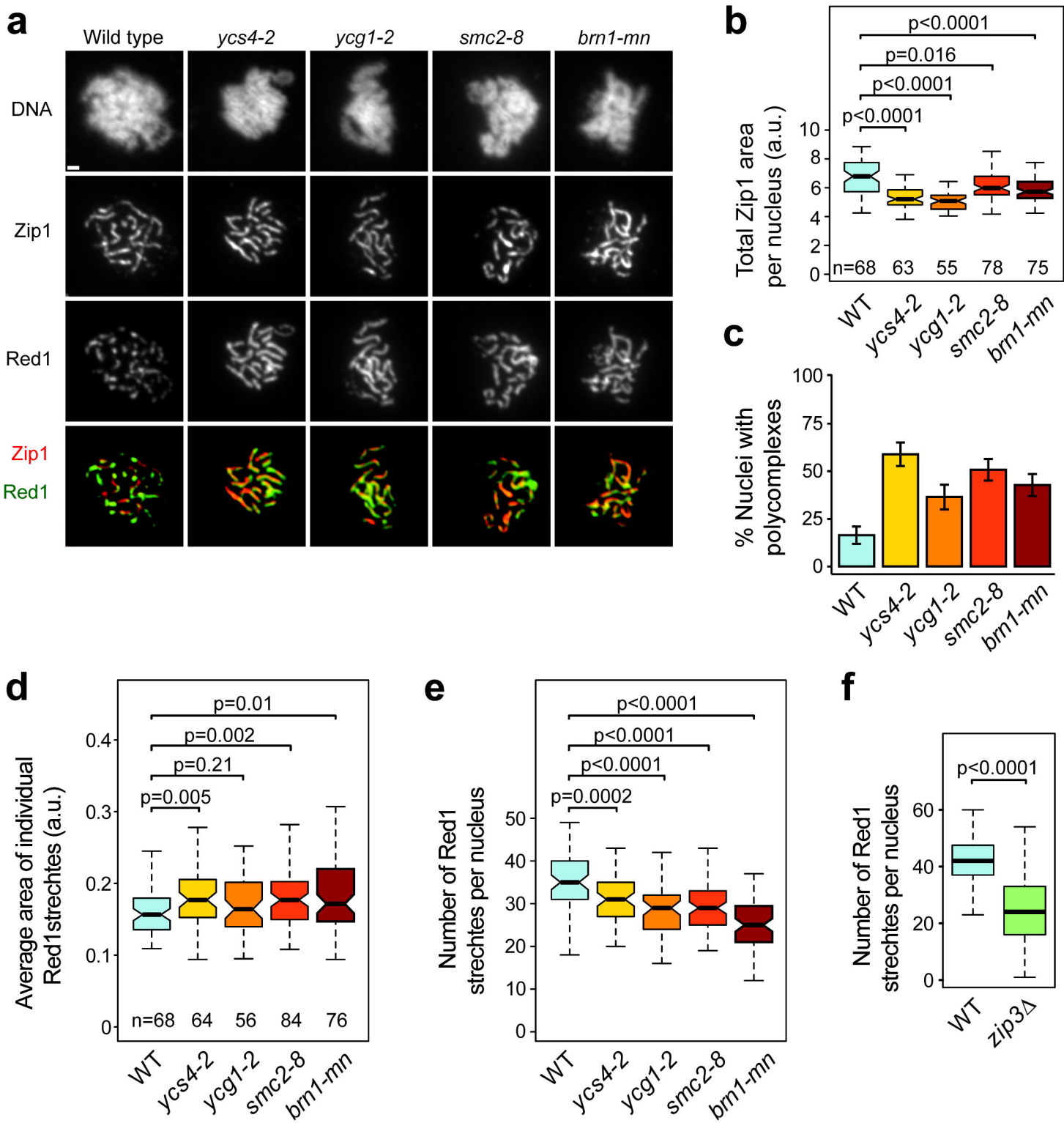

Leon et al, Figure 5

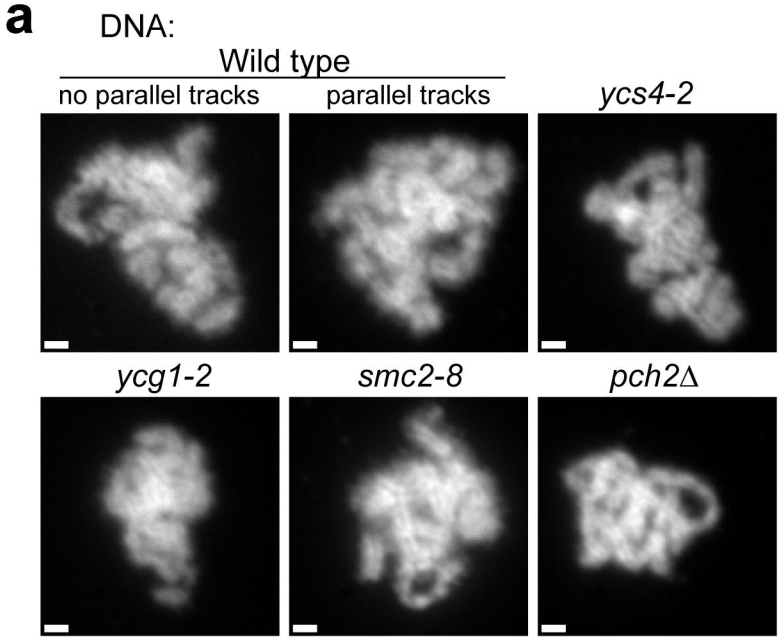

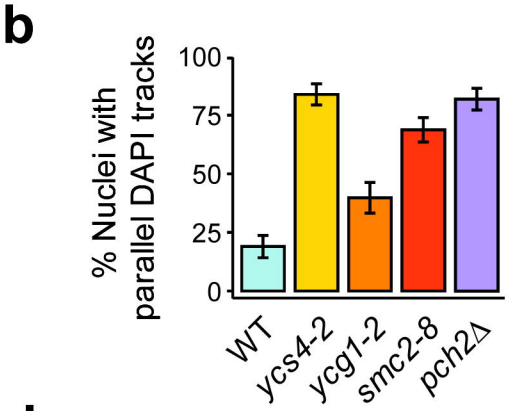

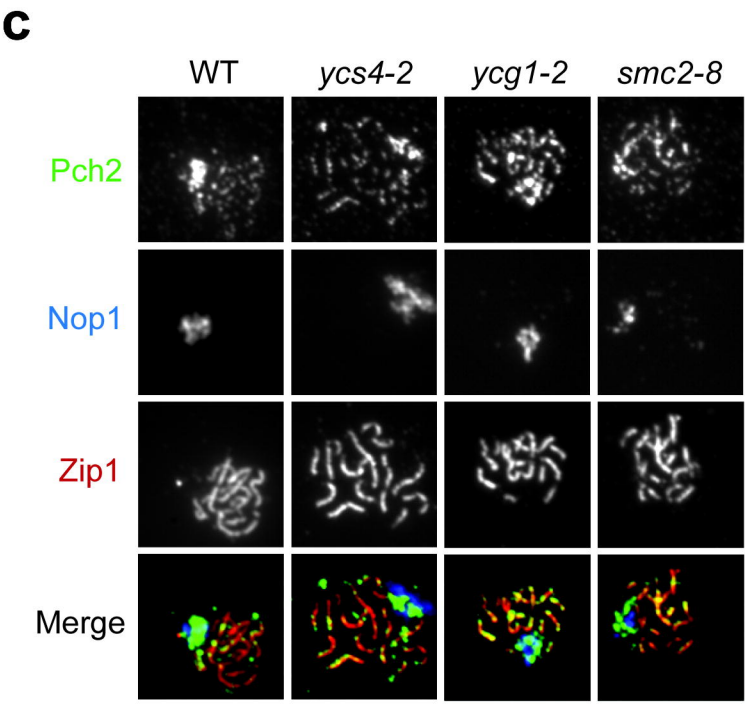

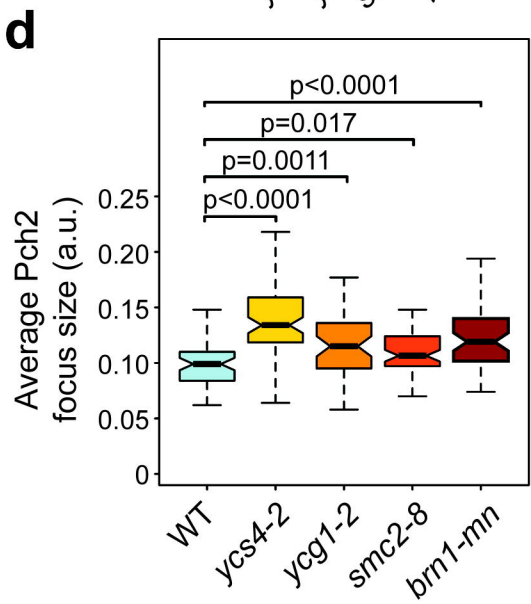

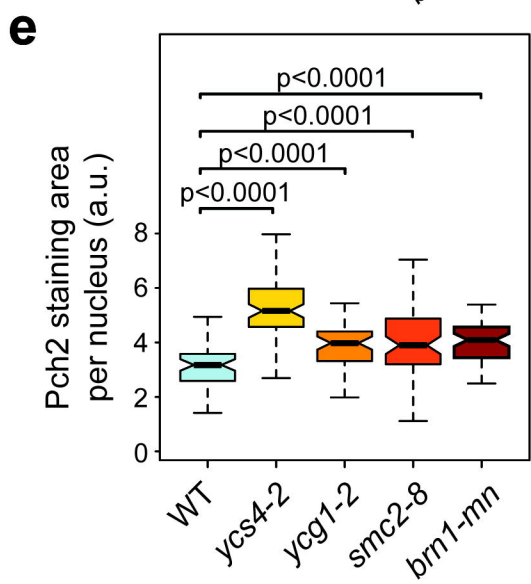

Leon et al, Figure 6

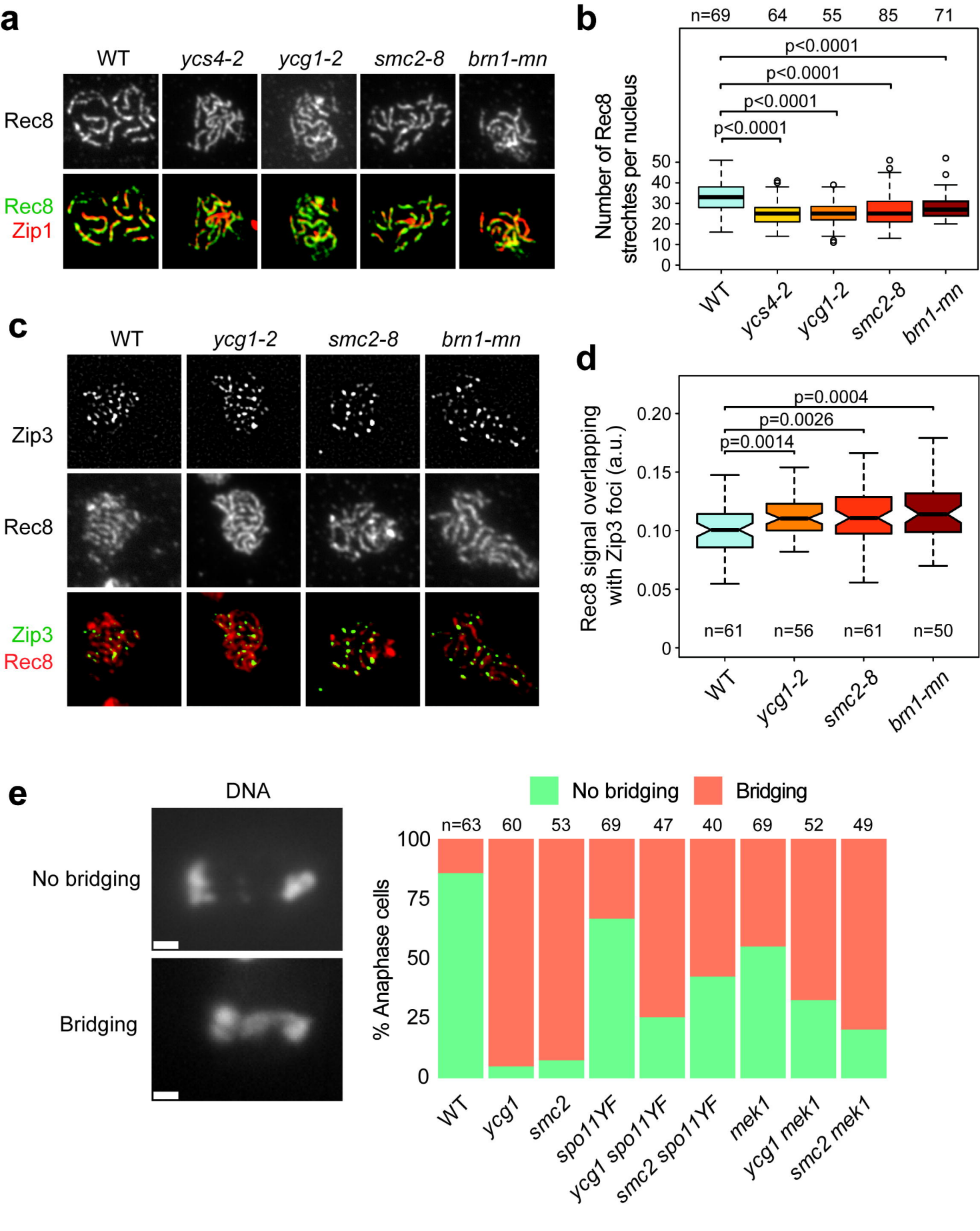

Leon et al, Figure 7